TMS provokes target-dependent intracranial rhythms across human cortical and subcortical sites

Authors

Ethan A. Solomon[1†], Jeffrey B. Wang[1,2], Hiroyuki Oya[3], Matthew A. Howard[3], Nicholas T. Trapp[4,5], Brandt D. Uitermarkt[6], Aaron D. Boes[4,5,6*], Corey J. Keller[1,7*]

Affiliations

[1] Dept. of Psychiatry and Behavioral Sciences, Stanford University Medical Center, Palo Alto CA 94305
[2] Biophysics Graduate Program, Stanford University Medical Center, Stanford, CA 94305
[3] Department of Neurosurgery, Carver College of Medicine, University of Iowa, Iowa City, IA, 52242
[4] Department of Neurology, Carver College of Medicine, University of Iowa, Iowa City, IA, 52242
[5] Department of Psychiatry, Carver College of Medicine, University of Iowa, Iowa City, IA, 52242
[6] Department of Pediatrics, Carver College of Medicine, University of Iowa, Iowa City, IA, 52242
[7] Veterans Affairs Palo Alto Healthcare System, and the Sierra Pacific Mental Illness, Research, Education, and Clinical Center (MIRECC), Palo Alto, CA, 94305

*Indicates co-last author with equal contributions.
†Correspondence may be addressed to esolom@stanford.edu.

Abstract

Transcranial magnetic stimulation (TMS) is increasingly deployed in the treatment of neuropsychiatric illness, under the presumption that stimulation of specific cortical targets can alter ongoing neural activity and cause circuit-level changes in brain function. While the electrophysiological effects of TMS have been extensively studied with scalp electroencephalography (EEG), this approach is most useful for evaluating low-frequency neural activity at the cortical surface. As such, little is known about how TMS perturbs rhythmic activity among deeper structures – such as the hippocampus and amygdala – and whether stimulation can alter higher-frequency oscillations. Understanding these effects is necessary to refine clinical stimulation protocols and better use TMS as a neuroscientific tool to investigate causal relationships in the brain. Recent work has established that TMS can be safely used in patients with intracranial electrodes (iEEG), making it possible to collect direct neural recordings at sufficient spatiotemporal resolution to examine oscillatory responses to stimulation. To that end, we recruited 17 neurosurgical patients with indwelling electrodes and recorded neural activity while patients underwent repeated trials of single-pulse TMS at various cortical sites. We found that TMS elicited widespread – but brief – changes in spectral power that markedly differed according to the stimulation target. Stimulation to the dorsolateral prefrontal cortex (DLPFC) drove widespread low-frequency increases (3-8Hz) in frontolimbic cortices, as well as high-frequency decreases (30-110Hz) in frontotemporal areas. Stimulation in parietal cortex specifically provoked low-frequency responses in the medial temporal lobe and hippocampus but not other regions. We also found high inter-trial phase consistency at low frequencies in the early post-stimulation period, suggestive of evoked responses. Taken together, we established that exogenous, non-invasive stimulation can be used to (1) provoke phase-locked theta increases and (2) briefly suppress high-frequency activity in a cortico-subcortical pattern that varies by stimulation target.

Introduction

Transcranial magnetic stimulation (TMS) has been heralded as a transformative technology in the treatment of neuropsychiatric illness. Through the induction of a magnetic field via a coil placed near the skull, TMS allows physicians to target specific brain regions and networks for modulation, completely non-invasively and often in outpatient clinical settings. Of particular interest has been its application in psychiatry, with a growing literature suggesting that TMS is effective for depression and may also be effective for bipolar, addiction, and other psychiatric disorders. More recently, investigators have reported that TMS delivered to individually-selected brain areas multiple times per day can yield rapid and sustained improvement in depressive symptoms[1,2].

These clinical successes suggest that repetitive stimulation of cortical targets may change neural activity at the circuit- or network-level of brain function. Evidence from non-invasive measures of neural activity support this claim. Investigators have long probed motor-evoked potentials[3], and more recently used fMRI BOLD[4] and scalp EEG[5,6] to characterize changes in TMS-induced neural activity and plasticity. In general, such studies found that repetitive TMS can alter cortical excitability by variably promoting long-term potentiation (LTP) or depression (LTD)-like effects – depending on the stimulation parameters[3,7] – as well as drive changes in neural activity in distant brain regions through functional or structural connections[8–11]. A hypothesized antidepressant effect of TMS, for example, arises from strengthened connectivity between the dorsolateral prefrontal cortex (DLPFC) and downstream regions within a cognitive-control network[2,12]. While foundational to our understanding of TMS neurophysiology, these non-invasive studies are fundamentally limited in their power to describe brain dynamics on the detailed spatiotemporal scale necessary to understand the neural effects of TMS and guide novel treatments.

A parallel line of research in neurosurgical patients has examined neural dynamics on a finer scale, leveraging the ability to electrically stimulate and record from intracranial electrodes (intracranial EEG; iEEG). Such indwelling electrodes record neural signals with precise spatial localization, high temporal resolution, low noise, and can access deep brain structures which are difficult to measure through scalp EEG[13]. In these studies, direct cortical electrical stimulation (DES) has been shown to provoke widespread, rhythmic changes in neural activity that appear similar to the spontaneous, endogenous oscillations which are crucial to sensory and cognitive processing[14–18]. Moreover, these effects are observed in deeper structures – like the hippocampus and amygdala – that play important roles in cognition and disease pathogenesis[17,19]. These studies also found that stimulation, like cognitive processes themselves, could provoke rhythmic activity in a sustained fashion, lasting at least several cycles of the frequency of interest.

Although neural oscillations are critical in neuropsychiatric disease, we have only a limited understanding of how TMS affects such oscillatory neural activity[17,18]. Studies which have combined scalp EEG recordings and TMS tend to focus on the brief evoked responses (termed TMS-evoked potentials, or TEPs[8,20–25]) and are limited in their ability to anatomically localize the origin of a neural event, particularly for areas far from the cortical surface[8,24–27]. A smaller number of studies attempted to differentiate the phase-locked “evoked” response from more sustained oscillations that occur with variable phase relation to the stimulus (also called “induced”), but making this distinction can be theoretically and methodologically ambiguous[28–31]. Additionally, scalp EEG offers unreliable estimates of oscillatory activity at higher frequencies

due to signal attenuation by the skull, muscle artifact, and the generally smaller spatial extent of higher-frequency signals[32].

Until recently, TMS in neurosurgical patients with indwelling electrodes was avoided for safety concerns, though new evidence suggests the approach is safe. Specifically, Wang and colleagues demonstrated that TMS does not displace, induce thermal changes, or elicit substantial changes in electrical fields in implanted electrodes. Moreover, they observed intracranial TMS-evoked potentials (iTEPs) in functionally connected regions that were downstream from a cortical target, demonstrating invasively-recorded neural responses to non-invasive stimulation[33,34]. While an important advance, this study did not evaluate the rich time-frequency information that can be extracted from intracranial electrodes with both high fidelity and spatiotemporal resolution. Such precise time-frequency information would allow investigators to tease out neural effects at specific frequencies of interest, a key physiological dimension which may be foundational to the brain's functioning[35,36].

To that end, we set out to characterize the full-spectrum oscillatory response of the human brain to TMS. We recruited 17 neurosurgical patients with indwelling cortical grids, strips, and depth electrodes while patients underwent repeated single-pulse trials of TMS. By comparing to sham stimulation, we quantified TMS-related oscillatory responses, particularly focusing on the theta (3-8Hz) and gamma (30-50Hz) bands that have been implicated in cognition and neuropsychiatric disease[37], as well as the high-frequency activity (HFA; 70-110Hz) range that likely reflects population spiking[38]. Our goals were to build on existing TMS-EEG and TMS-fMRI work by (1) understanding whether TMS can induce sustained oscillations, as opposed to brief evoked responses, and (2) examining the responses of subcortical structures to cortical stimulation.

We found that TMS was generally associated with strong, phase-locked, and widespread increases in low frequency power lasting less than 500ms following each pulse – likely reflective of the low frequency content of the iTEP. Regions that exhibited this response were sensitive to the stimulation site, with DLPFC stimulation driving low-frequency power in frontolimbic cortices and parietal stimulation driving medial temporal lobe (MTL) responses, including hippocampus. Moreover, DLPFC stimulation was associated with a post-stimulation suppression of gamma and HFA spectral power. Taken together, these results demonstrate that TMS can be used to modulate the neural activity of cortical and subcortical structures, most often increasing low-frequency power and suppressing high-frequency power.

Results

Combined TMS and iEEG allows for a detailed spectrotemporal analysis of TMS-related neurophysiology that is fundamentally inaccessible to non-invasive measurements. Briefly, we recruited 17 neurosurgical subjects with indwelling electrodes who underwent single-pulse active TMS (spTMS; *n*=50-150 trials, 0.5Hz) and sham (*n*=50-300 trials), targeting the DLPFC or parietal cortex (**Figure 1A**; see *Methods*). DLPFC was targeted at the individual level anatomically (Beam F3 method), while parietal sites were targeted at the individual level by the anatomical subregion with maximal resting state fMRI-based connectivity to the hippocampus[39] (see *Methods*). By statistically comparing the spectral power following sham and TMS pulses, we mapped the frequency-domain responses to stimulation across a wide array of intracranially-

recorded brain regions, including bilateral frontal, temporal, parietal, limbic, and medial temporal areas (**Figure 1B, 1C**).

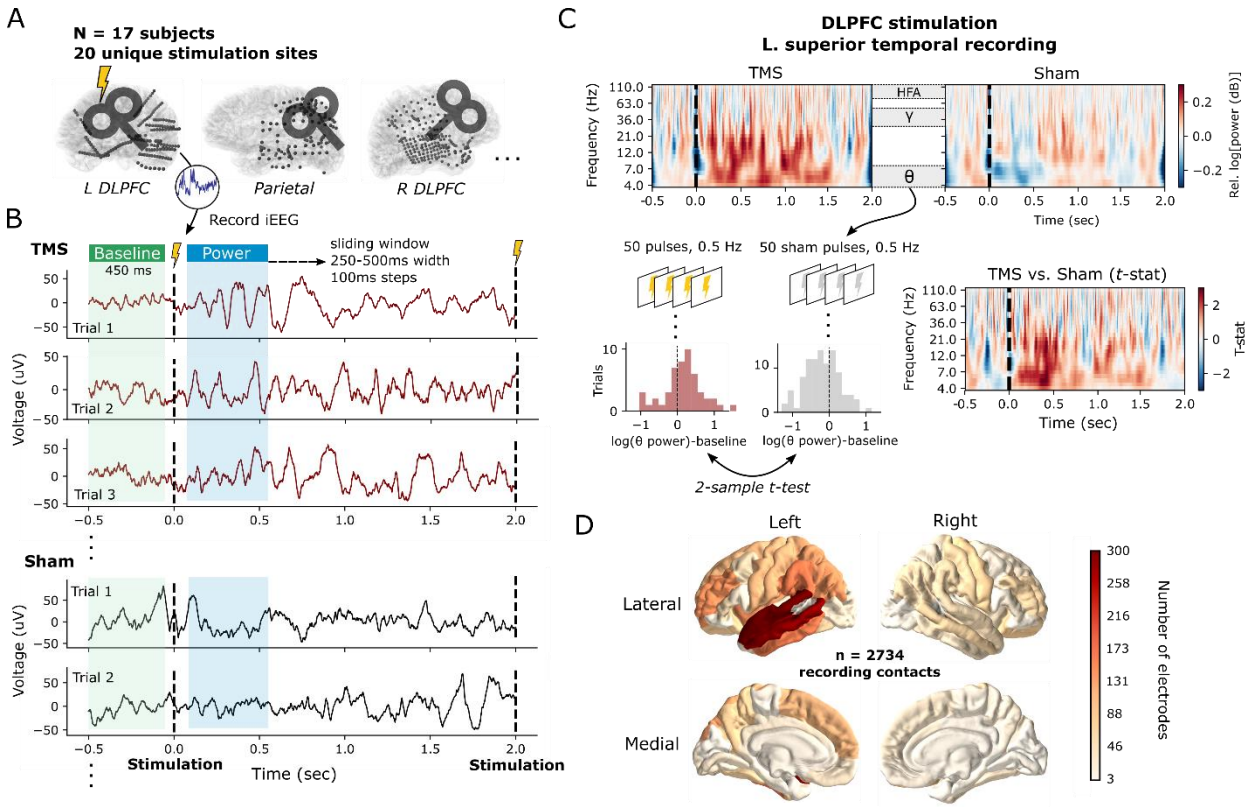

Figure 1. Stimulation protocol and analysis pipeline in an example subject. (A) Example schematic representations of the intracranial recording locations and stimulation locations in three subjects from the 17-subject dataset. **(B)** Data shown for one superior temporal gyrus (STG) stereo-EEG recording site recorded during TMS stimulation of the left DLPFC. For each stimulation site within a subject, single-pulse TMS is delivered at least 50 times with 2-second inter-stimulation intervals. In a separate block, at least 50 sham pulses are delivered by flipping the direction of the coil away from the skull, eliminating the induced electric field within the brain, while keeping other experimental parameters constant. For all recording contacts, intracranial EEG is simultaneously recorded and multitaper spectral power extracted in 500ms intervals (250ms for HFA to capture faster fluctuations) starting 50ms after the stimulation pulse (see *Methods* for details). To correct for changes in baseline power from trial-to-trial, power is also computed in a 450ms window preceding each stimulation event, and subtracted from post-stimulation power. **(C)** Example time-frequency spectrograms of the power response to TMS and sham stimulation (*top row*), derived from the same superior temporal gyrus iEEG data as in (B). Throughout this study, the power measured across TMS trials is statistically compared to the power following sham trials using a 2-sample *t*-test, generating a *t*-statistic which reflects the degree to which TMS increases or decreases oscillatory power relative to sham (*bottom row*). Sample data is shown for power extracted from the theta (3-8Hz) band within the first 500ms following stimulation. Full spectrograms are shown for completeness; statistical comparisons are rendered on data that excludes the stimulation pulse itself as described in (B). **(D)** Total count of recording contacts (n = 2374) for each Desikan-Killiany cortical parcellation in the 17-subject dataset.

Brain-wide spectral responses to DLPFC and parietal stimulation

We first took an overarching view of the brain's response to TMS, asking if significant differences between TMS and sham-related spectral power were observable in the theta, gamma, or HFA bands (**Supplemental Figure 1, Figure 2A-B**). By measuring spectral power in successive windows following stimulation (see *Methods*), we used linear mixed-effects modeling (LMM) to find significant early (starting 50ms-150ms post-stimulation in 500ms windows) increases in theta power from DLPFC stimulation, specifically in the frontal (Wald test, $z = 3.20$, $P = 0.001$, Intercept = [0.283, 1.179] 95% CI) and limbic cortices (Wald $z = 4.161$, $P < 0.001$, Intercept = [0.327, 0.910] 95% CI). This effect became nonsignificant in time windows starting 250ms after stimulation in both regions. A significant early (starting 50ms post-stimulation) theta response was also observed in the MTL following parietal stimulation, but not DLPFC stimulation (Wald $z = 3.75$, $P < 0.001$, Intercept = [0.199, 0.636] 95% CI). DLPFC stimulation had an anatomically broad, later (starting 250-450ms post-stimulation) suppression of activity in the gamma and HFA bands, which only survived FDR correction in the temporal cortex (Wald $z = -3.81$, $P < 0.001$, Intercept = [-0.50, -0.16] 95% CI). Of note, by using a windowed spectral approach beginning 50ms after stimulation, we avoid the possibility of direct contamination by the stimulation artifact itself.

As this global analysis averages across frequency bands and large time windows, it may obscure interesting dynamics that do not cleanly align with predefined time ranges. Within each of the theta-responsive regions identified above, we further analyzed each region by averaging the time-frequency responses across electrodes and subjects, testing each time-frequency "pixel" for a significant TMS vs. sham difference, and correcting for multiple comparisons (**Figure 2C**, $P < 0.05$; see *Methods*). This time-resolved analysis necessarily means stimulation artifact may contaminate power measures close to the pulse, though see *Methods* and *Discussion* for further considerations. Consistent with the previous analysis, these results demonstrate initial broadband power increases to DLPFC stimulation as recorded in frontal and limbic cortices, with the strongest effect in theta and alpha bands (approximately 4-13Hz). DLPFC stimulation suppressed alpha/beta (approximately 9-21Hz) power between 300-500ms post-stimulation in limbic regions. DLPFC stimulation also induced a long lasting (up to 1200ms) gamma and HFA suppression in frontal cortices. Furthermore, after DLPFC stimulation both limbic and frontal regions demonstrated a weaker, later (1-1.5s) increase in theta, alpha, and beta power. Finally, parietal stimulation provoked a significant early (0-400ms post-stimulation) theta and alpha-range increase in the MTL.

Taken together, these results align with prior noninvasive literature that suggest generally widespread and brief responses in lower frequencies to TMS[20,22,40], overlapping with the general spectral profile of TEPs (see *Inter-trial phase locking* for further analysis, as well as *Discussion*). We extend these findings by demonstrating that such responses are also observed in subcortical areas including MTL, and that regional responses are dictated by the targeted area. Most evidently, the MTL demonstrates a theta response to hippocampally-targeted parietal stimulation but no significant spectral response to DLPFC stimulation, even as widespread fronto-limbic cortices responded strongly.

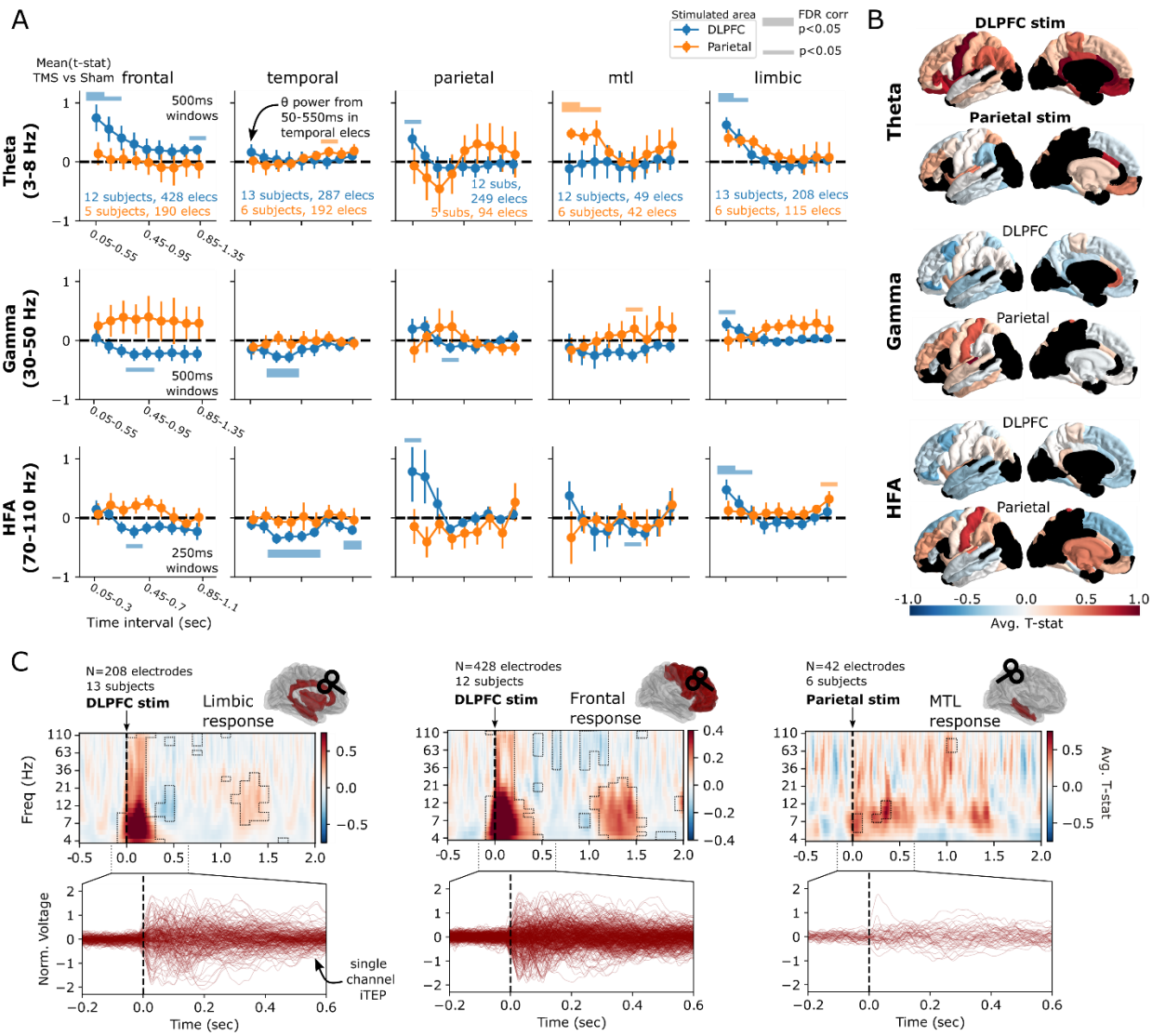

Figure 2. Differential regional responses to DLPFC versus parietal TMS. (A) For each frequency band (theta, gamma, and high-frequency activity [HFA]), spectral power is measured in 500ms (theta and gamma) or 250ms (HFA) windows across five 100ms steps, for every electrode and subject in the dataset. TMS-related power is statistically compared to sham-related power, as outlined in **Figure 1** and *Methods*. The resulting *t*-statistics are averaged across all electrodes within each subject, then across subjects, to generate curves reflecting the change in power over time. Significant differences between TMS and sham-related power are denoted with thick horizontal bars (*P*<0.05, FDR corrected over timepoints but not regions or frequencies). In the theta (3-8Hz) band, there is a significant early response in frontal cortices and limbic areas to DLPFC stimulation, while the MTL shows a significant early response to parietal stimulation. Temporal electrodes showed a significant gamma decrease in the intervals starting at 250-350ms, as well as a significant and sustained suppression of high-frequency activity (HFA; 70-110Hz). See **Supplemental Table 1** for a list of structures included in each area. Error bars show +/- 1 standard error of the mean over subjects (SEM). **(B)** Representation of average *t*-statistic for each ROI in the DKT atlas across all subjects and electrodes, in the 50-500ms (theta), 250-750ms (gamma), and 250-500ms (HFA) intervals. Black regions reflect areas with limited available data (fewer than 4 subjects). See **Supplemental Figure 2** for un-thresholded ROIs. **(C)** *Top:* For each of the three regions showing a significant theta response, time-frequency spectrograms were averaged across all

electrodes in each region, demonstrating brief (<500ms duration) increases in theta power immediately following stimulation, with lesser increases seen between 1-1.5 seconds post-stimulation. Boxed areas represent significant TMS vs. sham differences (P<0.05, FDR corrected). Time-frequency spectrograms were not generated for regions without a statistically significant theta response. *Bottom*: Butterfly plots representing the trial-averaged voltage response for each electrode across all subjects in a given region (i.e. an intracranially-recorded TEP, or iTEP).

Subcortical responses to cortical TMS

Subcortical structures play a key role in neuropsychiatric illness, but non-invasive electrophysiological recordings such as scalp EEG are unable to localize spectral activity from subcortical areas. Combined TMS-iEEG offers a unique opportunity to directly record from subcortical areas during concurrent TMS. In the previous analysis, we broadly demonstrated a low-frequency response to single pulse TMS in the MTL and limbic areas (**Figure 2**). We now examine the specific spectral dynamics which emerge in the hippocampus and amygdala – two areas which are (1) sufficiently sampled in our cohort (i.e. at least 5 subjects) and (2) strongly implicated in neuropsychiatric illnesses[41–43]. Our purpose is to characterize the full spectro-temporal responses to cortically-targeted TMS in these functionally and anatomically distinct structures, unlike our prior analysis of broad ROIs. In doing so, we hope to shed light on how propagated neural activity from the cortex manifests as subcortical rhythmic activity.

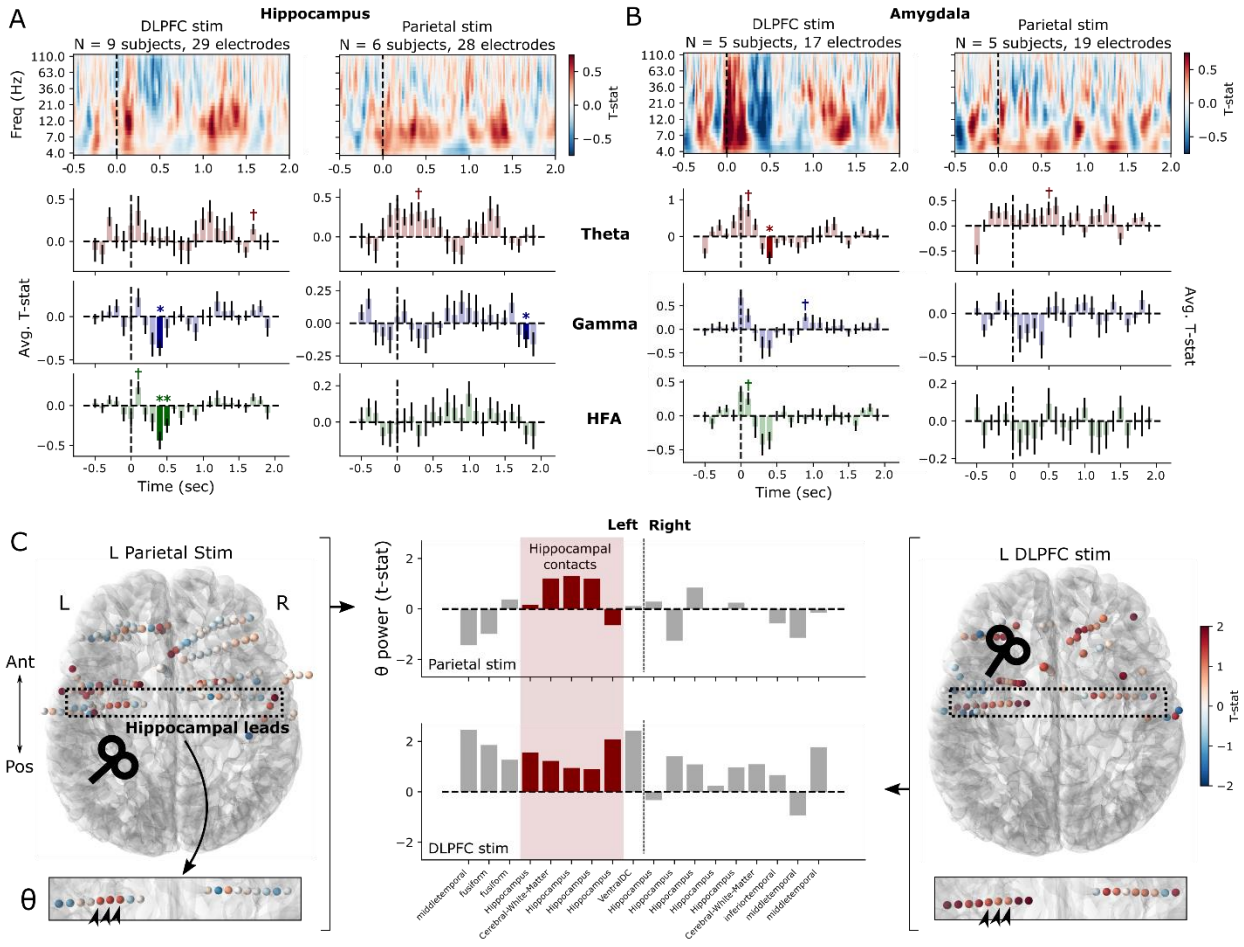

Figure 3. Subcortical responses to TMS in hippocampus and amygdala. (A) *Top:* Time-frequency spectrograms of the hippocampal response to DLPFC and parietal stimulation targeted towards the cortical area with maximal functional connectivity to the hippocampus. These reflect the average TMS-minus-sham difference across all electrodes and subjects; no statistical corrections are applied. Dotted line indicates time of stimulation pulse. *Bottom:* Timecourses of band-averaged power in the theta, gamma, and HFA bands, with indicators for significant TMS-minus-sham differences in 100ms windows (**P*<0.05, FDR corrected across timepoints, †*P*<0.05 uncorrected; see *Methods* for details). Error bars show +/- 1 SEM across contacts. **(B)** As in (A), but for amygdala spectral responses to DLPFC and parietal stimulation. **(C)** In a single subject who underwent both DLPFC and parietal stimulation, each recording contact is colored by the average theta power following TMS vs. sham stimulation (50-550ms post-stimulation). The hippocampal electrode leads were specifically examined (dotted box) to understand the differential responses in this structure to cortical stimulation. Theta power is represented for each recording contact along these leads (center bar plots) with hippocampal contacts highlighted in red. Three recording contacts (arrowheads) show a qualitatively increased response from parietal stimulation (left) which is less anatomically specific following DLPFC stimulation (right).

Averaged across all recording contacts and subjects, the hippocampus shows a significant suppression following DLPFC stimulation in the gamma band between 400 and 500ms post-stimulation (**Figure 3A**; Wald z = -3.4, P < 0.001) and HFA band between 400 and 600ms post-stimulation (z = -3.3, P < 0.001). (Nonsignificant increases in low-frequency power are appreciable principally in alpha and theta bands). No significant high-frequency suppression was observed after hippocampally-targeted parietal stimulation. However, a subthreshold

increase in theta power (i.e. $p < 0.05$ uncorrected; maximum of Wald $z = 2.1$ between 300-400ms) is seen in the first 500ms following parietal stimulation, which likely contributed to our earlier finding of theta power increases in the MTL more broadly. In the amygdala, a significant decrease in theta power was seen 400-500ms after DLPFC stimulation offset ($z = -3.5$, $P < 0.001$), alongside subthreshold early increases and later decreases in broadband spectral power. Parietal stimulation results in no significant spectral modulation in any band after correction for multiple comparisons (**Figure 3B**). The appearance of a broadband response within the amygdala to DLPFC stimulation raised the question of possible contamination by stimulation artifact. By examining the spectral responses of individual electrodes, the broadband-appearing response was rather driven by substantial inter-subject and inter-electrode variability in peak responses, which manifests as a broadband response in the statistical average – without evidence for contamination by stimulation artifact (**Supplemental Figure 3**).

Our use of hippocampally-targeted parietal stimulation – via rsfMRI functional connectivity – raises the question as to whether such targeted stimulation yields specific hippocampal responses. In general, as shown earlier, the MTL exhibits a significant low-frequency response to parietal stimulation which is not evident in DLPFC stimulation (**Figure 2A**). And on average, the hippocampus itself demonstrates a subthreshold increase in theta power following parietal, but not DLPFC stimulation (**Figure 3A**). Given the underlying heterogeneity of responses to TMS, we asked whether specific hippocampal responses were evident at the single-subject level (**Figure 3C**). Only two subjects received both DLPFC and parietal stimulation; one of those two demonstrated a qualitatively specific increase in hippocampal theta power in response to parietal stimulation, while exhibiting broad, nonspecific theta increases following DLPFC stimulation (which were lesser in magnitude in the hippocampus relative to ipsilateral cortical areas). The other subject did not demonstrate a qualitatively or quantitatively specific response in the hippocampus following parietal stimulation.

Given strong interest in the interplay between DLPFC and anterior cingulate cortex (ACC) – with prior evidence indicating that TMS can be used to alter ACC activity and connectivity[33,44] – we further analyzed the spectral response to DLPFC-targeted TMS in cingulate subregions (**Supplemental Figure 4**). The ACC as a whole showed a brief significant response in theta, gamma, and HFA bands from 100-200ms after stimulation ($p < 0.05$, FDR corrected). Upon inspecting ACC subregions, we found that the rostral ACC demonstrated a robust and statistically significant increase in theta power following TMS, persisting until 600ms post-stimulation. The caudal ACC showed no significant effect during that interval in theta, though continued to demonstrate significant early (100-200ms) increases in gamma and HFA. Posterior cingulate cortex (PCC) demonstrated no significant spectral modulation in any prespecified frequency band. (We qualitatively noted a suppression of alpha and low-beta power, approximately 9-15Hz, in the 250-500ms interval.) Of note, fewer than 5 subjects had parietally-targeted TMS and cingulate recording contacts, precluding analysis of cingulate response to parietal TMS.

Taken together, these analyses of subcortical responses in small-samples or individual subjects should be interpreted in their statistical context: early hints of the possibility that TMS can be used to modulate the spectral activity within subcortical structures. Specifically, there is a statistically reliable finding that DLPFC stimulation can drive suppression of high-frequency activity in the hippocampus and low-frequency activity in the amygdala. No statistically

significant effects emerge following parietal stimulation, but we found a notable increase in hippocampal theta power within 500ms of stimulation offset that does not reach corrected significance. As these sample sizes are small and may exhibit substantial inter-individual variability, further work is needed to validate whether this evidence is idiosyncratic, or reflects a repeatable means to non-invasively and predictably modulate subcortical rhythmic activity.

TMS influences inter-trial phase locking at low frequencies

Having established that TMS can alter spectral power in disparate brain regions – in part as a function of the stimulation region – we next asked if stimulation also exerts an effect on the phase of rhythmic activity. The phase of brain rhythms carries useful information about the nature of a rhythmic signal and may also reveal changes in brain dynamics that were not detectable by measuring changes in spectral power alone. Specifically, when interpreted alongside amplitude increases, the phase consistency of rhythms evoked by TMS helps characterize them as either “induced” or “evoked,” i.e. whether a stimulation pulse provokes rhythms with low or high phase consistency over trials, respectively[45]. In this study, we used the inter-trial phase locking metric (IPL), a commonly-used quantification of phase consistency across trials, computed for each individual electrode (see *Methods* for details). We focused on the theta (3-8Hz) band, which is well-established as containing cognitively and physiologically-relevant phase locking properties, especially relative to higher frequencies (e.g. gamma and higher)[46–48].

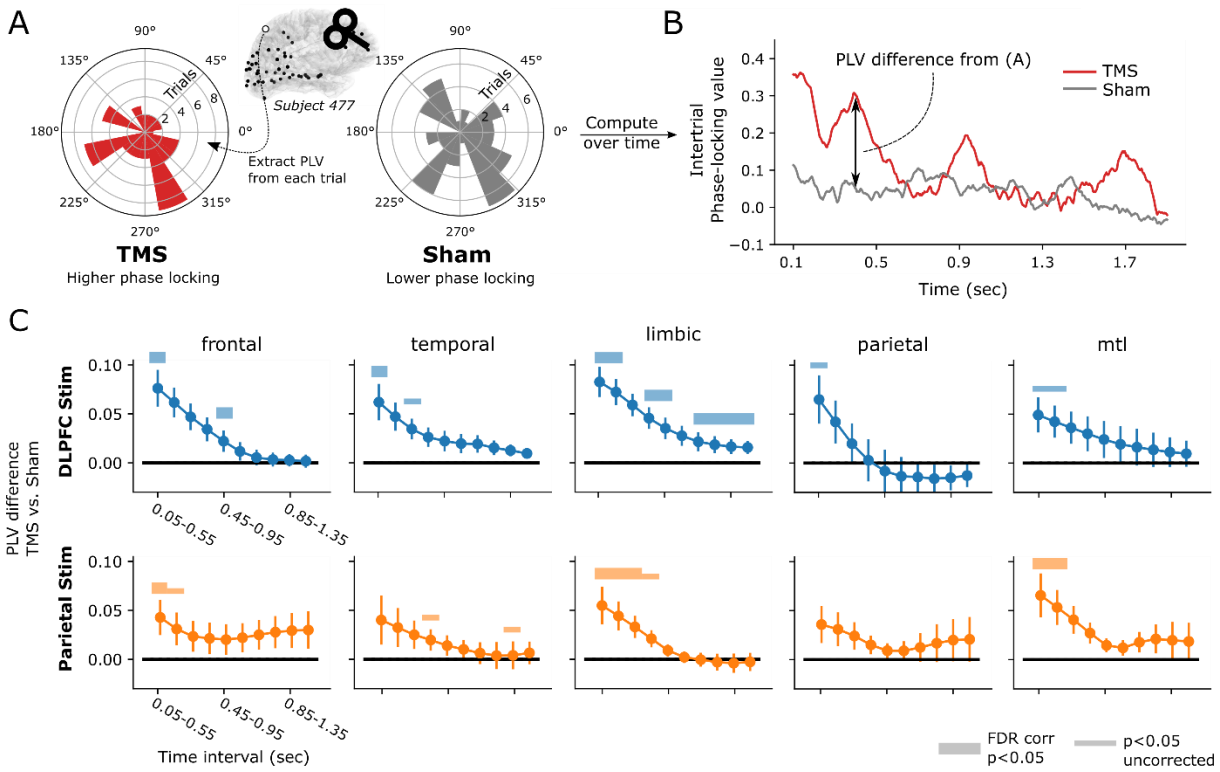

Figure 4. TMS-related theta (3-8 Hz) band inter-trial phase locking. (A) Schematic example of inter-trial phase locking value (PLV) computed at one superior parietal electrode from a representative subject, assessed at approximately 400ms after DLPFC stimulation. In this example, there is an elevated inter-trial phase locking in TMS trials – indicating a consistent theta phase across trials – which manifests as a circular phase distribution with clustering in a particular direction (i.e. to one side of the 0 degree axis). Sham trials exhibit a phase distribution with higher variance, corresponding to a lower PLV. **(B)** Timecourse of the PLV for TMS and sham trials from the electrode highlighted in (A). **(C)** Average TMS-minus-sham PLV difference across all subjects and electrodes for the same broad regions used in Figure 2, in 500ms windows spanning the post-stimulation period. Colored bars indicate timepoints when the PLV difference significantly differs from zero (linear mixed effects modeling, FDR corrected $P < 0.05$; see Methods for details). Frontal and limbic cortices show early increases in phase locking in TMS relative to sham trials for DLFPC and parietal stimulation. MTL regions show a significant early increase driven by parietal stimulation. In all regions, early increases in phase-locking decays towards zero by 1-second following stimulation; limbic cortices show a lower but significant TMS-driven increase in PLV that persists throughout the interval. Error bars show +/- 1 SEM across subjects. See **Figure 2A** for the count of subjects and electrodes for each stimulation-region combination.

Briefly, IPL was measured by extracting continuous theta-band phase in the post-stimulation time period, and then computing the phase-locking value (i.e. consistency of phase) across all trials for TMS and sham events, separately (**Figure 4A**). In doing so a continuous measure of the difference between TMS-IPL and Sham-IPL can be computed for each electrode (**Figure 4B**). By measuring the difference between TMS-IPL and Sham-IPL, and then averaging across electrodes into regions-of-interest, we derive a statistical measure of the TMS-related IPL, analogous to the power *t*-statistics shown earlier (**Figure 2**). Following DLPFC stimulation, we found that, across broad ROIs, there is significant TMS-related IPL provoked across several

areas, though effects only survive multiple comparisons correction in the frontal, temporal, and limbic ROIs (**Figure 4C top row**; frontal: Wald $z = 4.7$, $P < 0.001$; temporal: $z = 3.13$, $P = 0.002$; limbic: $z = 4.94$, $P < 0.001$). In frontal and temporal cortices, the effect is strongest and only significant in the early post-stimulation period (frontal: 50ms and 450ms intervals; temporal: 50ms interval). The effect is significant for most of the first second following stimulation in limbic cortices, though nonetheless decays monotonically over this interval. Parietal and MTL cortices show no FDR-corrected significant TMS-related change in IPL with DLPFC stimulation.

Following parietal stimulation, effects are similarly early and rapidly decay (**Figure 4C, bottom row**). Significant effects (FDR-corrected $P < 0.05$) are only found in frontal (starting at 50ms; Wald $z = 3.16$, $P = 0.002$), limbic (starting at 50-350ms; $z = 2.64$, $P = 0.008$), and MTL areas (starting at 50-150ms; $z = 2.72$, $P = 0.007$). Similar to DLPFC, these regions show a steady decay in TMS-minus-sham IPL that tends to approach zero around 500ms post-stimulation.

Discussion

TMS is used to modulate neural circuits in neuropsychiatric illness, but until recently, human brain responses to stimulation could only be understood by non-invasive, spatiotemporally imprecise methods. In this study, we used indwelling electrodes to measure intracranial responses to TMS, allowing for signals that are more precise and have higher spatiotemporal resolution that can be decomposed in the full spectral domain. In doing so, we aimed to (1) characterize the spectral responses of key brain regions to TMS, focusing on three major frequency bands of interest (theta, gamma, HFA), and (2) examine the responses of deep brain structures to TMS, shedding light on how downstream regions respond to propagated activity from stimulated cortex.

We found that DLPFC stimulation tended to cause brief, early increases in theta power in frontal and limbic cortices, particularly the anterior cingulate cortex (ACC; **Supplemental Figure 4**). Higher frequencies, including gamma and HFA bands, were suppressed predominantly in the temporal lobe, though smaller effects were also noted frontally. Parietal stimulation – which was targeted based on functional connectivity to the hippocampus – caused significant early theta increases in the MTL, but in no other regions or frequency bands. In the hippocampus, DLPFC stimulation attenuated high-frequency activity, while parietal stimulation increased low-frequency activity. In almost all cases, spectral effects were isolated to the first 500ms following stimulation, and this time period was also associated with significant theta-band inter-trial phase locking in the same regions that exhibited increases in theta power.

Taken together, these results demonstrate that TMS reliably provokes brain-wide changes in spectral power across frequency bands, and the effects are specific to the location of stimulation. Predictably, functionally-targeted parietal stimulation provoked qualitatively greater responses in the MTL/hippocampus as compared to frontal stimulation (**Figure 2A, 3C**), though we had insufficient data to statistically measure this effect within-subjects. This is suggestive that functional connections dictate the way in which stimulation propagates through the brain, extending a growing body of literature[14,49–51]. However, further work is needed to determine if this principle generalizes to other stimulation sites and recording areas. Moreover, as our focus was to characterize modulations of region-specific power and phase locking, we did not ascertain whether individual variability in functional connectivity correlates with the effect of

stimulation in downstream regions. To answer both of these questions, we plan to analyze the relationship between subject-specific measures of intracranial functional connectivity (e.g. resting-state fMRI or electrophysiological coherence) and the TMS-provoked activity recorded at indwelling electrodes.

From these data, it is also clear that non-invasive, cortically-targeted stimulation can modulate electrical activity in deep brain structures that are not directly accessed by stimulation itself, extending previous work in direct cortical stimulation[52,53] and fMRI[9,54]. Within the limits of the moderately-sized samples in this study (up to 17 subjects depending on the stimulation site and recording location), our data suggest that TMS directed at the DLPFC – at least following single pulses – suppresses high-frequency activity in the hippocampus for several hundred milliseconds. There is also weak but intriguing evidence that parietal stimulation can instigate theta rhythms in the hippocampus – a finding that has profound implications for how we might use stimulation in modulating core cognitive functions of the hippocampus itself[39,55,56]. Although the mapping between stimulation and amygdala responses is less clear, these results highlight the potential for using TMS to precisely modulate the function of deep brain structures with profound implication in neuropsychiatric disease. Future work should focus on clarifying how cortically-propagated signals exert their effects on these structures, and whether specific stimulation patterns can be used to provoke specific frequency responses[57].

Our results are consistent with prior evidence from combined TMS and scalp-EEG[5,24,25], serving to replicate and build upon our understanding of TMS physiology. Specifically, these results support the notion that single-pulse TMS tends to cause brief, cortically-distributed potentials in the theta to alpha range, typically less than 500ms in duration, with a predictable and consistent phase locking to the stimulation event itself. This phase consistency – and the brief duration – would categorize such potentials as *evoked* rather than *induced* (which would instead suggest prolonged, ongoing oscillations at a particular frequency with variable phase relationship to the stimulus)[58]. Though there is longstanding speculation about the physiological or cognitive relevance of this distinction[45], it should be emphasized that both phenomena are rhythmic fluctuations in local field potentials, and the presence of one does not strictly exclude the other. Indeed, the spectral analyses in this paper do not rule out the presence of sustained oscillations that occur at the subject- or electrode-level but not in grand averages.

To better tease out these distinct neural phenomena, future work should focus on two relevant directions. First, there is a possibility that alternative stimulation paradigms – such as repetitive or rhythmic (e.g. theta-burst) stimulation – would provoke induced as opposed to evoked rhythmic activity. Prior work examining the cortical responses to patterned direct intracranial stimulation suggest this would be the case by demonstrating prolonged power increases or non-timelocked events[15,18,59–61], though this remains to be established with TMS. Second, as noted above, the statistical methods used here relied on aggregate effects, generally at the level of broad ROIs. While such an approach is reasonable to reduce spurious findings in an exploratory-style analysis, it may obscure dynamics that occur within specific subjects or particular subregions. Though speculative, there are hints of such phenomena in our data here, where hippocampal (and ACC) responses to TMS demonstrated more sustained effects in the theta band which do not reach corrected significance (**Figure 3A**, **Supplemental Figure 4**).

TMS-induced neural effects in high-frequency bands are also consistent with prior non-invasive work[18,61,62], and intracranial observation of these findings with higher signal-to-noise enhance their biological validity. Moreso than the low-frequency increases, early (200-500ms) decreases

in gamma and HFA were consistent and statistically significant in widespread regions following DLPFC stimulation, especially in frontal and temporal cortices (including medial temporal regions). These frequency bands have been hypothesized as signatures of population neural spiking, particularly in high gamma and HFA[38]. Accordingly – because HFA relates to neural firing – our findings suggest a TMS-related suppression of neural firing. This effect may be either directly related to the TMS pulse itself or indirectly as an aftereffect of the low-frequency evoked potential. The effect in hippocampus is particularly notable, as these dynamics could not be reliably elucidated with non-invasive measures or without the high temporal resolution of iEEG. The ability to predictably suppress neural firing in the hippocampus with cortically-targeted TMS could point towards its therapeutic potential, especially in psychiatric illness that features pathological hippocampal activity, such as depression[63] or psychosis[64].

Stimulation-response paradigms often raise the question of spectral contamination by the pulse artifact. While it is difficult to ensure that zero artifactual components enter these kinds of analyses, several features of our analytic methods and results suggest the effect would be small. First, our core analyses in **Figure 2A** and **Figure 4C** used windowed measures of spectral power that contain no data from the stimulation period itself, beginning 50ms after stimulation offset. To subsequently provide a fuller spectral representation of stimulation's effects in specific areas, time-frequency representations in **Figure 2C** and **Figure 3A-B** necessarily do overlap with the stimulation interval. However, care was taken to remove and re-interpolate the stimulation artifact period, as described in *Methods* – our demonstration of peak effects more than 100ms after stimulation suggests that this data cleaning was successful. Finally, we demonstrated decreases in high-frequency power starting several hundred milliseconds (e.g. **Figure 3A**) after stimulation, which would be very unlikely to occur due to stimulation artifact alone.

These findings represent a key advance in how we understand the mechanisms of TMS-related change in neural function. More broadly, they demonstrate the promise of combining non-invasive stimulation with direct intracranial recordings, providing a window into the detailed electrophysiology of brain stimulation while developing a therapeutic technique that can be easily deployed in outpatient clinical settings.

Methods

Human subjects

Seventeen neurosurgical patients with medically intractable epilepsy underwent a surgical procedure to implant intracranial recording contacts on the cortical surface (electrocorticography) and within brain parenchyma (stereo-EEG). Contacts were placed in accordance with clinical need to localize epileptic regions. Each patient was admitted to the University of Iowa Hospitals and Clinics for 14 days of clinical and electrophysiological monitoring to identify their seizure focus. TMS experiments were conducted after the final surgical treatment plan was agreed upon between the clinical team and the patient, typically 1-2 days before the planned electrode explantation operation and 24 hours after the patient had restarted anti-epileptic medications. All experimental procedures were approved by the University of Iowa Institutional Review Board, who reviewed safety data from a separate experiment prior to approval for human subjects[33].

Imaging protocol and intracranial electrode localization

Intracranial electrodes were localized in a manner identical to that described in Wang, et al. (2022)[33]. Briefly, patients underwent anatomical and functional MRI scans within two weeks of electrode implantation, including resting-state functional MRI (rsfMRI). The day following implantation, subjects underwent a second MRI and volumetric computerized tomography (CT) scans. The location of each contact was identified on the post-implantation T1-weighted MRI and CT, and subsequently post-implantation scans were transformed to pre-implantation T1 anatomical space in a manner that accounts for the possibility of post-surgical brain shift[65]. Freesurfer[66] was used to map electrode locations onto a standardized set of coordinates across subjects, which were then labeled according to their location within the Desikan-Killiany-Tourville (DKT) anatomical atlas.

Transcranial magnetic stimulation

For stimulation, we used a MagVenture MagVita X100 230V system with a figure-of-eight liquid-cooled Cool-B65 A/P coil (Magventure; Alpharetta, GA, USA). Stimulation pulses were biphasic sinusoidals with a pulse width of 290 microseconds, with stimulator output set at a percentage of each subject's motor threshold. Pulses were delivered at 0.5Hz, allowing for 2-second inter-stimulation intervals to examine spectral responses. TMS experiments were conducted 12-13 days after implantation and after starting antiepileptic medications. Neuronavigation using frameless stereotaxy was guided with Brainsight software supplied with the pre-implantation T1/MPRAGE anatomical scan. Stimulation parameters were recorded in Brainsight during all experimental trials. Motor thresholds were determined starting with the hand knob of the motor cortex as a target, beginning at 30% machine output and adjusted in 5-10% increments until movements were observed in 50% of trials.

In the main experiment, single pulses were directed at DLPFC or parietal targets at or above motor threshold (100% was used if 120% was not tolerated due to pain). DLPFC targets were defined by the Beam F3 region[67], identified by transforming published coordinates (MNI 1mm: -41.5, 41.1, 33.4)[68] into each subject's native T1 and displaying it in Brainsight. The stimulation site was adjusted slightly if access was impeded by head wrap or anchor bolts for securing electrodes. Parietal targets were identified by localizing the site within the inferior parietal lobe with maximal resting-state fMRI-based connectivity to the hippocampus. A 4mm spherical ROI was placed at the contact location in the hippocampus to serve as the seed. Mean timecourse in the ROI was calculated, and then a Pearson's correlation against this timecourse was calculated for every voxel to generate a simple network map. This correlation map was then loaded into Brainsight and thresholded to identify the highest correlation in the lateral parietal cortex posterior to the post-central gyrus, visually confirmed to be the peak correlated voxel nearest to the lateral parietal ROI published in Nilakantan et al. (2019)[69].

Sham pulses were delivered in an identical manner to active, with the TMS coil flipped 180 degrees such that the magnetic field was directed away from the head. Participants underwent at least 50 stimulation pulses ("trials") and 50 sham pulses, though we included subjects with as many as 150 stimulation and 300 sham events, if time and clinical constraints allowed. In one subject, only 33 single pulse TMS trials were included due to tolerability.

iEEG recording

Electrode recordings were conducted in a manner identical to Wang, et al. (2022)[33]. Briefly, depth and grid electrodes (Ad-Tech Medical; Racine, WI, USA) were either stereotactically implanted or placed on the cortical surface, respectively. A platinum-iridium strip electrode placed in the midline subgaleal space was used as a reference. Data were amplified, filtered (ATLAS, Neuralynx, Bozeman MT; 0.7-800 Hz bandpass), and digitized at 8000Hz. In all subjects, contacts were excluded from analysis if they were determined to be involved in the generation or early propagation of seizures (412/3894 contacts; 10.6%), if stimulation artifact saturated the amplifier (835/3894; 21.4%), or if electrodes were contaminated by nonneural noise indicative of poor connection or placement outside the brain (67/3894; 1.7%).

iEEG preprocessing and analysis

The FieldTrip MATLAB toolbox[70] was used to load iEEG data into our analysis pipeline. Data preprocessing analysis was principally done with the MNE toolbox[71] in Python. First, raw signals were re-referenced to account for large-scale noise or contamination of the reference electrodes; stereo-EEG (depth) electrodes were re-referenced using a bipolar montage, while grids and strips on the cortical surface were collectively re-referenced to their common average.

Although we generally avoided performing spectral analysis on the period of time containing the ~15ms stimulation artifact itself, some analyses (including generation of time-frequency representations in **Figure 2** and **Figure 3**) necessitate analysis of the full interval during each trial. For this reason, we scrubbed the stimulation artifact from all signals and replaced it with synthesized stationary iEEG that reflects a similar spectral profile as the background[72]. Specifically, the iEEG signal was clipped from 25 ms prior to 25 following stimulation and replaced with a weighted average of the 50ms immediately following and prior to stimulation. Specifically, the pre- and post-stimulation clips were first reversed, then tapered linearly to zero along the length of the signal, and then finally summed together to replace the artifact period. Finally, signals were notch filtered at 60 Hz and harmonics to remove line noise, using an F-test to find and remove sinusoidal components[73]. Lastly, signals were downsampled to 500 Hz for further analysis.

Our general analytic strategy was to statistically compare spectral activity in TMS trials against sham trials, in order to control for auditory and expectancy effects associated with the stimulation click. To do this, iEEG signals for each contact were segmented into 2.5-second intervals, spanning 500ms prior to stimulation until 2 seconds following stimulation (**Figure 1B**). To first examine broad effects in the large ROIs used in **Figure 2**, we used the multitaper method (time-bandwidth product of 4, excluding tapers with <90% spectral concentration) to measure the power spectral density (PSD) from 3Hz to 110Hz in discrete 500ms or 250ms windows, depending on the frequency of interest. 500ms windows were used in the theta (3-8 Hz) and gamma (30-50 Hz) ranges, while 250ms windows were utilized for high-frequency activity (HFA; 70-110Hz). These differential widths account for the fact that high-frequency activity tends to fluctuate at faster timescales than power in lower frequency bands, making it more appropriate to analyze in briefer time windows. Power was estimated starting 50ms after

stimulation to avoid residual contamination from stimulation artifact, in successive overlapping windows spaced 100ms apart until 850ms following stimulation.

Power responses in large ROIs and subcortical areas

In each time window and for each frequency band, powers were log-transformed and averaged over constituent frequencies within the band. To account for drifts in baseline power over time, we subtracted "baseline" power as measured in a 450ms window preceding each stimulation event, buffered by a 50ms gap from the stimulation artifact to avoid any chance of contamination (**Figure 1B**). Baseline power was otherwise measured exactly as per spectral methods described above (*iEEG preprocessing and analysis*). Baseline-corrected powers were compared between TMS trials and sham trials using a two sample *t*-test. This process generated a *t*-statistic for each recording contact in the dataset, at each timepoint and frequency band of interest. Finally, *t*-statistics were averaged across all contacts that fell within a given ROI, for every subject. We did not analyze any region with less than 5 subjects' worth of data for a given stimulation target.

To generate **Figure 2A**, *t*-statistics were averaged across subjects and tested against zero for significance. Due to the hierarchical nature of our data, variable number of electrodes in each subject, and the possibility of correlated responses between electrodes within subject, we adopted a linear mixed modeling approach (LMM) for major statistical analyses in this manuscript. Specifically, we used the LMM implementation in the Python statsmodels package[74]. Here, we used intercept-only LMMs to model the variability of *t*-statistics across recording contacts and subjects, specifying subjects as random effects. We used the Wald test to assess the significance of the intercept, asking whether power *t*-statistics significantly differed from zero in our population. Resulting *p*-values were FDR corrected for multiple comparisons over timepoints ($\alpha = 0.05$). Note that, in **Figure 2A**, error bars reflect +/- 1 standard error the mean (SEM) over subjects, as the hierarchical variability discussed above cannot be easily graphically represented.

To generate the time-frequency spectrograms in **Figure 2C** and **Figure 3A-B**, we slightly modified our analytic approach to allow for the continuous measurement of spectral power, as opposed to discrete windows (**Figure 1B, 2A**). For each contact, we used the Morlet wavelet convolution (3 cycles in length) to extract a continuous measure of power at 25 log-spaced frequencies between 3Hz and 110Hz, log-transformed the result, and subtracted baseline power in the manner described above. We used a 2-sample *t*-test to compare powers between TMS and sham trials, at each pixel of the time-frequency representation. To test for statistical significance of regions within the time-frequency representation (**Figure 2C**), *t*-statistics for each contact in a given ROI were first averaged within subjects, and then tested against zero using 1-sample *t*-tests to generate a *p*-value for each pixel; finally, *p*-values were FDR corrected for multiple comparisons ($\alpha = 0.05$) to identify time-frequency areas where TMS-related neural activity significantly different from sham activity.

We note that, in using a continuous measure of power over the entire trial, these time-frequency representations may reflect contamination from stimulation artifact, despite efforts to reduce this effect (see *iEEG preprocessing and analysis*). For this reason, our primary statistical analyses

were performed on windowed intervals that strictly avoid samples which could contain stimulation artifact (**Figure 2A**).

Analytic methods to measure spectral power in the hippocampus and amygdala (**Figure 3A-B**) were generally identical to those described above. However, to quantify the specific temporal dynamics of how spectral power evolved in these regions after the TMS pulse, we avoided the 500ms windows used to assess large-scale power dynamics as in **Figure 2**. Instead, we first performed Morlet wavelet convolution and then averaged resulting powers into successive non-overlapping 100ms windows, for each frequency band. Statistical testing for significant differences between TMS and sham trials was performed using the same LMM approach as outlined above. Given the smaller number of subjects and electrodes which contributed to these regions, we did not perform statistical testing on the time-frequency representations themselves.

Inter-trial phase locking (IPL)

To assess the effect of TMS on low-frequency phase locking, we adopted the inter-trial phase locking (IPL) metric, otherwise known as the phase-locking value[75]. This metric reflects the consistency of phase values, at a given frequency and timepoint, across all trials. High IPL would be indicative of rhythms that are significantly phase-locked to the stimulation pulse, whereas low IPL cannot be concretely interpreted (either reflecting low amplitude rhythms, non-phase locked rhythms, or some combination of both). As for our initial power computations, we again used the multitaper method (time-bandwidth product of 4, two cycles in length, spanning 3-8Hz) as implemented in MNE Python ("tfr_array_multitaper"), which computes IPL by first extracting a continuous measure of phase, and then measures the inter-trial consistency by measuring the mean resultant vector length of phase values across trials. Resulting IPLs fall between 0 and 1, with 1 indicating perfectly consistent phases across trials, and 0 indicating phase distributed uniformly from 0 to 360 degrees.

Since phase-locking is biased by the number of trials that contribute to its computation[58], we randomly selected *n* trials from the TMS and sham events in each subject, where *n* is the lower number of trials between the two blocks. In this way, trial counts were matched across TMS and sham events, removing the possibility of PLV bias. IPL was measured starting 50ms after stimulation, similar to our power analyses. As IPL is sensitive to edge artifact, we applied a 450ms "mirror" buffer to the edges of the signal before convolution by reversing the leading and trailing edges of the signal. These buffers were then clipped from the resulting IPL trace prior to further analysis. Finally, as in our power analyses, we measured average IPL In the 450ms "baseline" period prior to each stimulation event (see *Power responses in large ROIs and subcortical areas*), and subtracted this value from post-stimulation IPL for each trial. To measure the TMS-related IPL relative to sham-related IPL, we subtracted the (baseline-corrected) sham IPL from TMS IPL to generate a difference measure (ΔIPL), where positive values would reflect TMS-related increases in inter-trial phase locking.

As in our power analyses, we measured the population effect of TMS on IPL (**Figure 4**) by first averaging ΔIPL for each in 500ms windows spanning the post-stimulation period, beginning at 50ms following stimulation and ending at 850ms in 100ms steps. Next, we averaged ΔIPLs across all contacts within a given ROI, and finally averaged across subjects. As described previously, we used an LMM approach to test the significance of ΔIPL in our population,

specifying subjects as random effects in an intercept-only model. *P*-values determined via a Wald test for significance were FDR corrected for multiple comparisons (α = 0.05), though we also show uncorrected *P*<0.05 for transparency (**Figure 4**).

Acknowledgements

First, we thank the neurosurgical patients who selflessly participated in this research. We thank Joel Bruss for assistance with imaging analyses. We also thank Christopher Kovach, Ariane Rhone, Haiming Chen, and Benjamin Pace for their assistance with image processing, coordinating, and conducting the experiments. This research was supported by NIMH R01MH132074 (CJK and ADB), R21MH120441 (ADB) and 5R01dC004290-20. EAS was supported by the Stanford Research-Track Psychiatry Residency Program. JBW was supported by F30MH119763 and the Mark and Mary Stevens Interdisciplinary Graduate 660 Fellowship. CJK was supported by R01MH132074, R01MH126639, R01MH129018, and a Burroughs Wellcome Fund Career Award for Medical Scientists. ADB. was also supported by R01NS114405. NTT was supported by 5T32-MH019113. This work was conducted, in part, on an MRI instrument funded by 1S10OD025025-01.

Author Contributions

EAS, JBW, HO, CJK, and ADB conceived of the study. EAS and JBW performed electrophysiology analyses. HO performed safety testing and analyses and participated in experimental testing with TMS. BDU and NTT participated in experimental testing. MH assisted with study design, safety, and subject recruitment. All authors contributed to the writing of the manuscript. ADB and CJK jointly supervised all aspects of the study. All authors have seen and approved the manuscript, and it has not been accepted or published elsewhere.

Competing Interests

CJK holds equity in Alto Neuroscience, Inc. EAS has previously received compensation for ad-hoc technical consulting for Nia Therapeutics, a company intended to develop and commercialize brain stimulation therapies. No other conflicts of interest, financial or otherwise, are declared by the authors.

References

1. Cole, E. J. *et al.* Stanford Neuromodulation Therapy (SNT): A Double-Blind Randomized Controlled Trial. *https://doi.org/10.1176/appi.ajp.2021.20101429* **179**, 132–141 (2021).

2. Philip, N. S., Barredo, J., Aiken, E. & Carpenter, L. L. Neuroimaging Mechanisms of Therapeutic Transcranial Magnetic Stimulation for Major Depressive Disorder. *Biol Psychiatry Cogn Neurosci Neuroimaging* **3**, 211–222 (2018).

3. Ziemann, U. *et al.* Consensus: Motor cortex plasticity protocols. *Brain Stimul* **1**, 164–182 (2008).

4. Bestmann, S. *et al.* Mapping causal interregional influences with concurrent TMS–fMRI. *Experimental Brain Research 2008 191:4* **191**, 383–402 (2008).

5. Rogasch, N. C. & Fitzgerald, P. B. Assessing cortical network properties using TMS–EEG. *Hum Brain Mapp* **34**, 1652 (2013).

6. Daskalakis, Z. J., Farzan, F., Radhu, N. & Fitzgerald, P. B. Combined transcranial magnetic stimulation and electroencephalography: Its past, present and future. *Brain Res* **1463**, 93–107 (2012).

7. Hoogendam, J. M., Ramakers, G. M. J. & Di Lazzaro, V. Physiology of repetitive transcranial magnetic stimulation of the human brain. *Brain Stimul* **3**, 95–118 (2010).

8. Eshel, N. *et al.* Global connectivity and local excitability changes underlie antidepressant effects of repetitive transcranial magnetic stimulation. *Neuropsychopharmacology* **45**, 1018–1025 (2020).

9. Hermiller, M. S., Chen, Y. F., Parrish, T. B. & Voss, J. L. Evidence for immediate enhancement of hippocampal memory encoding by network-targeted theta-burst stimulation during concurrent fMRI. *Journal of Neuroscience* **40**, 7155–7168 (2020).

10. Kim, S. *et al.* Selective and coherent activity increases due to stimulation indicate functional distinctions between episodic memory networks. *Sci Adv* **4**, (2018).

11. Bonato, C., Miniussi, C. & Rossini, P. M. Transcranial magnetic stimulation and cortical evoked potentials: a TMS/EEG co-registration study. *Clin Neurophysiol* **117**, 1699–1707 (2006).

12. Fischer, A. S., Keller, C. J. & Etkin, A. The Clinical Applicability of Functional Connectivity in Depression: Pathways Toward More Targeted Intervention. *Biol Psychiatry Cogn Neurosci Neuroimaging* **1**, 262–270 (2016).

13. Pesaran, B. *et al.* Investigating large-scale brain dynamics using field potential recordings: Analysis and interpretation. *Nat Neurosci* **21**, 903–919 (2018).

14. Keller, C. J. *et al.* Intrinsic functional architecture predicts electrically evoked responses in the human brain. *Proc Natl Acad Sci U S A* **108**, 10308–13 (2011).

15. Solomon, E. A. *et al.* Theta-burst stimulation entrains frequency-specific oscillatory responses. *Brain Stimulation: Basic, Translational, and Clinical Research in Neuromodulation* **14**, 1271–1284 (2021).

16. Solomon, E. A. *et al.* Medial temporal lobe functional connectivity predicts stimulation-induced theta power. *Nat Commun* **9**, 4437 (2018).

17. Keller, C. J. *et al.* Induction and quantification of excitability changes in human cortical networks. *The Journal of Neuroscience* 1088–17 (2018) doi:10.1523/JNEUROSCI.1088-17.2018.

18. Huang, Y. *et al.* Intracortical dynamics underlying repetitive stimulation predicts changes in network connectivity. doi:10.1101/548180.

19. Solomon, E. *et al.* Theta-burst stimulation entrains frequency-specic oscillatory responses. (2021) doi:10.21203/rs.3.rs-308421/v1.

20. Gogulski, J. *et al.* Mapping cortical excitability in the human dorsolateral prefrontal cortex. *bioRxiv* (2023) doi:10.1101/2023.01.20.524867.

21. Ross, J. M., Cline, C. C., Sarkar, M., Truong, J. & Keller, C. J. Neural effects of TMS trains on the human prefrontal cortex. *bioRxiv* (2023) doi:10.1101/2023.01.30.526374.

22. Wu, W. *et al.* ARTIST: A fully automated artifact rejection algorithm for single-pulse TMS-EEG data. *Hum Brain Mapp* **39**, 1607–1625 (2018).

23. Kerwin, L. J., Keller, C. J., Wu, W., Narayan, M. & Etkin, A. Test-retest reliability of transcranial magnetic stimulation EEG evoked potentials. *Brain Stimul* **11**, 536–544 (2018).

24. Ross, J. M., Sarkar, M. & Keller, C. J. Experimental suppression of transcranial magnetic stimulation-electroencephalography sensory potentials. *Hum Brain Mapp* **43**, 5141–5153 (2022).

25. Parmigiani, S. *et al.* Reliability and Validity of Transcranial Magnetic Stimulation-Electroencephalography Biomarkers. *Biol Psychiatry Cogn Neurosci Neuroimaging* (2022) doi:10.1016/J.BPSC.2022.12.005.

26. Kerwin, L. J., Keller, C. J., Wu, W., Narayan, M. & Etkin, A. Test-retest reliability of transcranial magnetic stimulation EEG evoked potentials. *Brain Stimul* **11**, 536–544 (2018).

27. Hernandez-Pavon, J. C. *et al.* TMS combined with EEG: Recommendations and open issues for data collection and analysis. *Brain Stimulation: Basic, Translational, and Clinical Research in Neuromodulation* **0**, (2023).

28. Premoli, I. *et al.* The impact of GABAergic drugs on TMS-induced brain oscillations in human motor cortex. *Neuroimage* **163**, 1–12 (2017).

29. Pellicciari, M. C., Veniero, D. & Miniussi, C. Characterizing the Cortical Oscillatory Response to TMS Pulse. *Front Cell Neurosci* **11**, 38 (2017).

30. Vallesi, A. *et al.* Natural oscillation frequencies in the two lateral prefrontal cortices induced by Transcranial Magnetic Stimulation. *Neuroimage* **227**, 117655 (2021).

31. Rosanova, M. *et al.* Natural frequencies of human corticothalamic circuits. *J Neurosci* **29**, 7679–7685 (2009).

32. Hipp, J. F. & Siegel, M. Dissociating neuronal gamma-band activity from cranial and ocular muscle activity in EEG. *Front Hum Neurosci* **7**, 338 (2013).

33. Wang, J. B. *et al.* Effects of transcranial magnetic stimulation on the human brain recorded with intracranial electrocorticography: First-in-human study. *bioRxiv* 2022.01.18.476811 (2022) doi:10.1101/2022.01.18.476811.

34. Boes, A. *et al.* Effects of transcranial magnetic stimulation on the human brain revealed by intracranial electrocorticography. *Brain Stimulation: Basic, Translational, and Clinical Research in Neuromodulation* **12**, 419 (2019).

35. Buzsáki, G. The Hippocampo-Neocortical Dialogue. *Cerebral Cortex* **6**, 81–92 (1996).

36. Buzsáki, G. & Draguhn, A. Neuronal Oscillations in Cortical Networks. *Science (1979)* **304**, (2004).

37. Godsil, B. P., Kiss, J. P., Spedding, M. & Jay, T. M. The hippocampal–prefrontal pathway: The weak link in psychiatric disorders? *European Neuropsychopharmacology* **23**, 1165–1181 (2013).

38. Manning, J. R., Jacobs, J., Fried, I. & Kahana, M. J. Broadband shifts in local field potential power spectra are correlated with single-neuron spiking in humans. *J Neurosci* **29**, 13613–20 (2009).

39. Wang, J. X. *et al.* Targeted enhancement of cortical-hippocampal brain networks and associative memory. *Science (1979)* **345**, 1054–1057 (2014).

40. Lioumis, P., Kičić, D., Savolainen, P., Mäkelä, J. P. & Kähkönen, S. Reproducibility of TMS—Evoked EEG responses. *Hum Brain Mapp* **30**, 1387–1396 (2009).

41. Harrison, P. J. The hippocampus in schizophrenia: A review of the neuropathological evidence and its pathophysiological implications. *Psychopharmacology* vol. 174 151–162 Preprint at https://doi.org/10.1007/s00213-003-1761-y (2004).

42. Kim, M. J. *et al.* The structural and functional connectivity of the amygdala: From normal emotion to pathological anxiety. *Behavioural Brain Research* vol. 223 403–410 Preprint at https://doi.org/10.1016/j.bbr.2011.04.025 (2011).

43. Grupe, D. W. & Nitschke, J. B. Uncertainty and anticipation in anxiety: an integrated neurobiological and psychological perspective. *Nature Reviews Neuroscience 2013 14:7* **14**, 488–501 (2013).

44. Mitra, A., Raichle, M. E., Geoly, A. D., Kratter, I. H. & Williams, N. R. Targeted neurostimulation reverses a spatiotemporal biomarker of treatment-resistant depression. *Proc Natl Acad Sci U S A* **120**, e2218958120 (2023).

45. David, O., Kilner, J. M. & Friston, K. J. Mechanisms of evoked and induced responses in MEG/EEG. *Neuroimage* **31**, 1580–1591 (2006).

46. Yamaguchi, Y. *et al.* A unified view of theta-phase coding in the entorhinal–hippocampal system. *Curr Opin Neurobiol* **17**, 197–204 (2007).

47. O'Keefe, J. & Recce, M. L. Phase relationship between hippocampal place units and the EEG theta rhythm. *Hippocampus* **3**, 317–330 (1993).

48. Shadlen, M. N. & Movshon, J. A. Synchrony Unbound: A Critical Evaluation of the Temporal Binding Hypothesis. *Neuron* **24**, 67–77 (1999).

49. Solomon, E. A. *et al.* MTL functional connectivity predicts stimulation-induced theta power. *bioRxiv* 320663 (2018) doi:10.1101/320663.

50. Fox, K. C. R. *et al.* Intrinsic network architecture predicts the effects elicited by intracranial electrical stimulation of the human brain. *Nat Hum Behav* **4**, 1039–1052 (2020).

51. Fox, M. D., Buckner, R. L., White, M. P., Greicius, M. D. & Pascual-Leone, A. Efficacy of Transcranial Magnetic Stimulation Targets for Depression Is Related to Intrinsic Functional Connectivity with the Subgenual Cingulate. *Biol Psychiatry* **72**, 595–603 (2012).

52. Mégevand, P. *et al.* The Hippocampus and Amygdala Are Integrators of Neocortical Influence: A CorticoCortical Evoked Potential Study. *Brain Connect* **7**, 648 (2017).

53. Ezzyat, Y. *et al.* Closed-loop stimulation of temporal cortex rescues functional networks and improves memory. *Nat Commun* **9**, 365 (2018).

54. Nilakantan, A. S., Bridge, D. J., Gagnon, E. P., VanHaerents, S. A. & Voss, J. L. Stimulation of the Posterior Cortical-Hippocampal Network Enhances Precision of Memory Recollection. *Current Biology* **27**, (2017).

55. Herweg, N. A., Solomon, E. A., Kahana, M. J. & Kahana, M. J. Theta Oscillations in Human Memory. *Trends Cogn Sci* **xx**, 20 (2019).

56. Buzsáki, G. Theta Oscillations in the Hippocampus. *Neuron* **33**, 325–340 (2002).

57. Suppa, A. *et al.* Ten Years of Theta Burst Stimulation in Humans: Established Knowledge, Unknowns and Prospects. *Brain Stimulation* vol. 9 323–335 Preprint at https://doi.org/10.1016/j.brs.2016.01.006 (2016).

58. Cohen, M. X. *Analyzing Neural Time Series Data*. *Analyzing Neural Time Series Data* (The MIT Press, 2014). doi:10.7551/mitpress/9609.001.0001.

59. Bentley, J. N. *et al.* Subcortical Intermittent Theta-Burst Stimulation (iTBS) Increases Theta-Power in Dorsolateral Prefrontal Cortex (DLPFC). *Front Neurosci* **14**, 41 (2020).

60. Noh, N. A., Fuggetta, G., Manganotti, P. & Fiaschi, A. Long Lasting Modulation of Cortical Oscillations after Continuous Theta Burst Transcranial Magnetic Stimulation. *PLoS One* **7**, e35080 (2012).

61. Keller, C. J. *et al.* Induction and Quantification of Excitability Changes in Human Cortical Networks. *J Neurosci* **38**, 5384–5398 (2018).

62. Farzan, F. *et al.* Suppression of γ-Oscillations in the Dorsolateral Prefrontal Cortex following Long Interval Cortical Inhibition: A TMS–EEG Study. *Neuropsychopharmacology 2009 34:6* **34**, 1543–1551 (2008).

63. Mayberg, H. S. Targeted electrode-based modulation of neural circuits for depression. *J Clin Invest* **119**, 717 (2009).

64. Lee, K. H., Williams, L. M., Breakspear, M. & Gordon, E. Synchronous Gamma activity: A review and contribution to an integrative neuroscience model of schizophrenia. *Brain Research Reviews* vol. 41 57–78 Preprint at https://doi.org/10.1016/S0165-0173(02)00220-5 (2003).

65. Oya, H. *et al.* Mapping effective connectivity in the human brain with concurrent intracranial electrical stimulation and BOLD-fMRI. *J Neurosci Methods* **277**, 101–112 (2017).

66. Fischl, B. FreeSurfer. *Neuroimage* **62**, 774–781 (2012).

67. Beam, W., Borckardt, J. J., Reeves, S. T. & George, M. S. An efficient and accurate new method for locating the F3 position for prefrontal TMS applications. *Brain Stimul* **2**, 50–54 (2009).

68. Fried, P. J., Rushmore, R. J., Moss, M. B., Valero-Cabré, A. & Pascual-Leone, A. Causal evidence supporting functional dissociation of verbal and spatial working memory in the human dorsolateral prefrontal cortex. *Eur J Neurosci* **39**, 1973–1981 (2014).

69. Nilakantan, A. S. *et al.* Network-targeted stimulation engages neurobehavioral hallmarks of age-related memory decline. *Neurology* **92**, e2349–e2354 (2019).

70. Oostenveld, R., Fries, P., Maris, E. & Schoffelen, J. M. FieldTrip: Open source software for advanced analysis of MEG, EEG, and invasive electrophysiological data. *Comput Intell Neurosci* **2011**, (2011).

71. Gramfort, A. *et al.* MNE software for processing MEG and EEG data. *Neuroimage* **86**, 446–460 (2014).

72. Crowther, L. J. *et al.* A quantitative method for evaluating cortical responses to electrical stimulation. *J Neurosci Methods* **311**, 67–75 (2019).

73. Dynamics, O. B. Oxford Scholarship Online Electrophysiology : Microelectrode Recordings. 1–38 (2009).

74. Seabold, S. & Perktold, J. *Statsmodels: Econometric and Statistical Modeling with Python*. *PROC. OF THE 9th PYTHON IN SCIENCE CONF* http://statsmodels.sourceforge.net/ (2010).

75. Lachaux, J. P., Rodriguez, E., Martinerie, J. & Varela, F. J. Measuring phase synchrony in brain signals. *Hum Brain Mapp* **8**, 194–208 (1999).

A

N = 17 subjects
20 unique stimulation sites

L DLPFC

Parietal

R DLPFC

Record iEEG

B

TMS

Baseline

450 ms

Power

sliding window
250-500ms width
100ms steps

Trial 1

Trial 2

Trial 3

Voltage (uV)

Sham

Trial 1

Trial 2

Stimulation

Stimulation

Time (sec)

C

DLPFC stimulation
L. superior temporal recording

TMS

Sham

Frequency (Hz)

HFA

γ

θ

Rel. log[power (dB)]

Time (sec)

50 pulses, 0.5 Hz

50 sham pulses, 0.5 Hz

Trials

log(θ power)-baseline

log(θ power)-baseline

2-sample t-test

TMS vs. Sham (*t*-stat)

Frequency (Hz)

Time (sec)

T-stat

D

Left

Right

Lateral

Medial

n = 2734
recording contacts

Number of electrodes

A

Stimulated area: DLPFC, Parietal

FDR corr p<0.05

p<0.05

Mean(t-stat) TMS vs Sham

frontal | temporal | parietal | mtl | limbic

Theta (3-8 Hz)

500ms windows

θ power from 50-550ms in temporal elecs

12 subjects, 428 elecs
5 subjects, 190 elecs

13 subjects, 287 elecs
6 subjects, 192 elecs

12 subs, 249 elecs
5 subs, 94 elecs

12 subjects, 49 elecs
6 subjects, 42 elecs

13 subjects, 208 elecs
6 subjects, 115 elecs

0.05-0.55 | 0.45-0.95 | 0.85-1.35

Gamma (30-50 Hz)

500ms windows

0.05-0.55 | 0.45-0.95 | 0.85-1.35

HFA (70-110 Hz)

250ms windows

0.05-0.3 | 0.45-0.7 | 0.85-1.1

Time interval (sec)

B

Theta

DLPFC stim

Parietal stim

Gamma

DLPFC

Parietal

HFA

DLPFC

Parietal

-1.0 -0.5 0.0 0.5 1.0

Avg. T-stat

C

N=208 electrodes
13 subjects
DLPFC stim
Limbic response

N=428 electrodes
12 subjects
DLPFC stim
Frontal response

N=42 electrodes
6 subjects
Parietal stim
MTL response

Freq (Hz)

Norm. Voltage

single channel iTEP

Time (sec)

Avg. T-stat

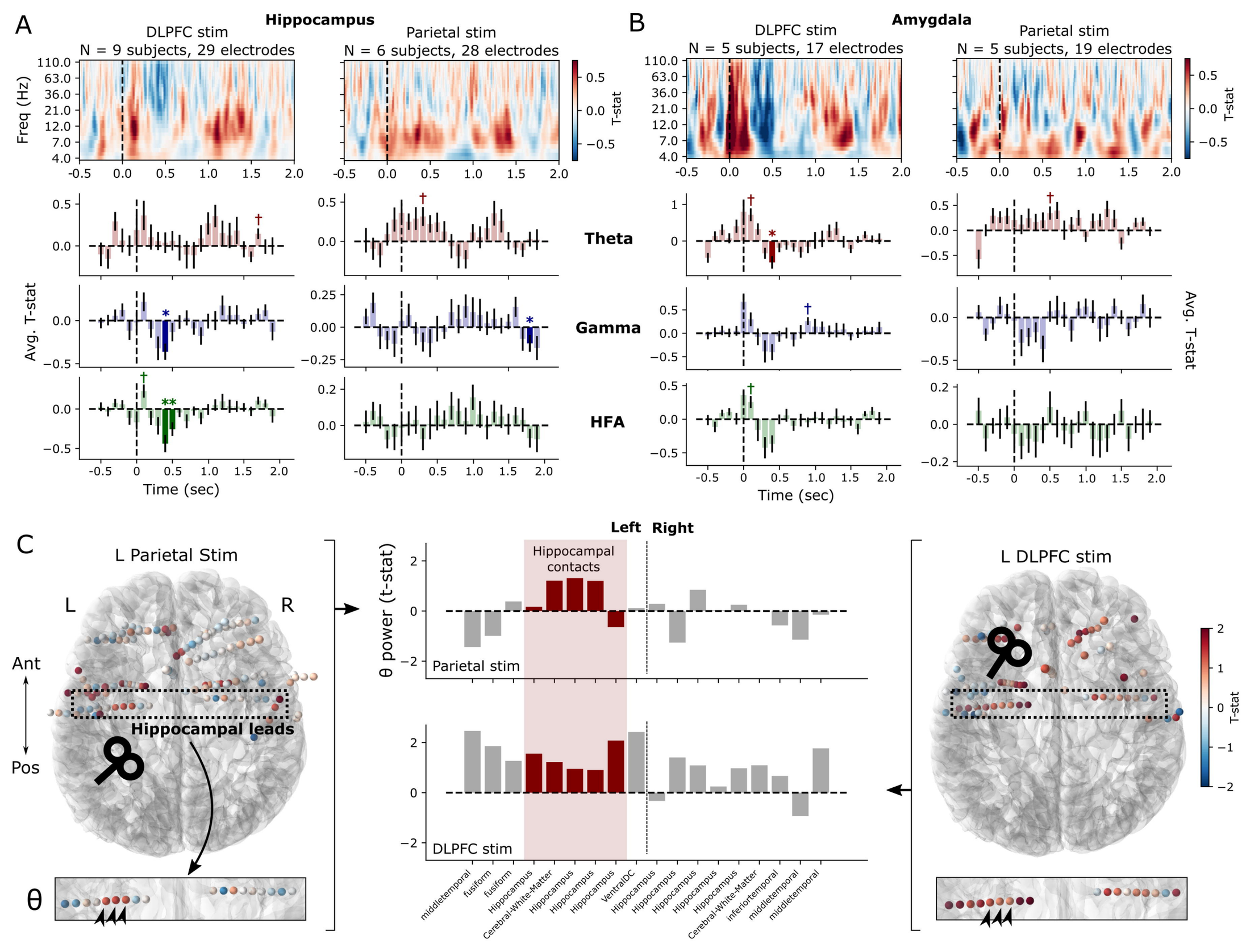
A
Hippocampus
DLPFC stim
N = 9 subjects, 29 electrodes
Parietal stim
N = 6 subjects, 28 electrodes
Freq (Hz)
T-stat
B
Amygdala
DLPFC stim
N = 5 subjects, 17 electrodes
Parietal stim
N = 5 subjects, 19 electrodes
Theta
Gamma
HFA
Avg. T-stat
Time (sec)
C
L Parietal Stim
L
R
Ant
Pos
Hippocampal leads
θ
Left Right
θ power (t-stat)
Hippocampal contacts
Parietal stim
DLPFC stim
middletemporal
fusiform
fusiform
Hippocampus
Cerebral-White-Matter
Hippocampus
Hippocampus
Hippocampus
VentralDC
Hippocampus
Hippocampus
Hippocampus
Hippocampus
Hippocampus
Cerebral-White-Matter
inferiortemporal
middletemporal
middletemporal
L DLPFC stim
T-stat

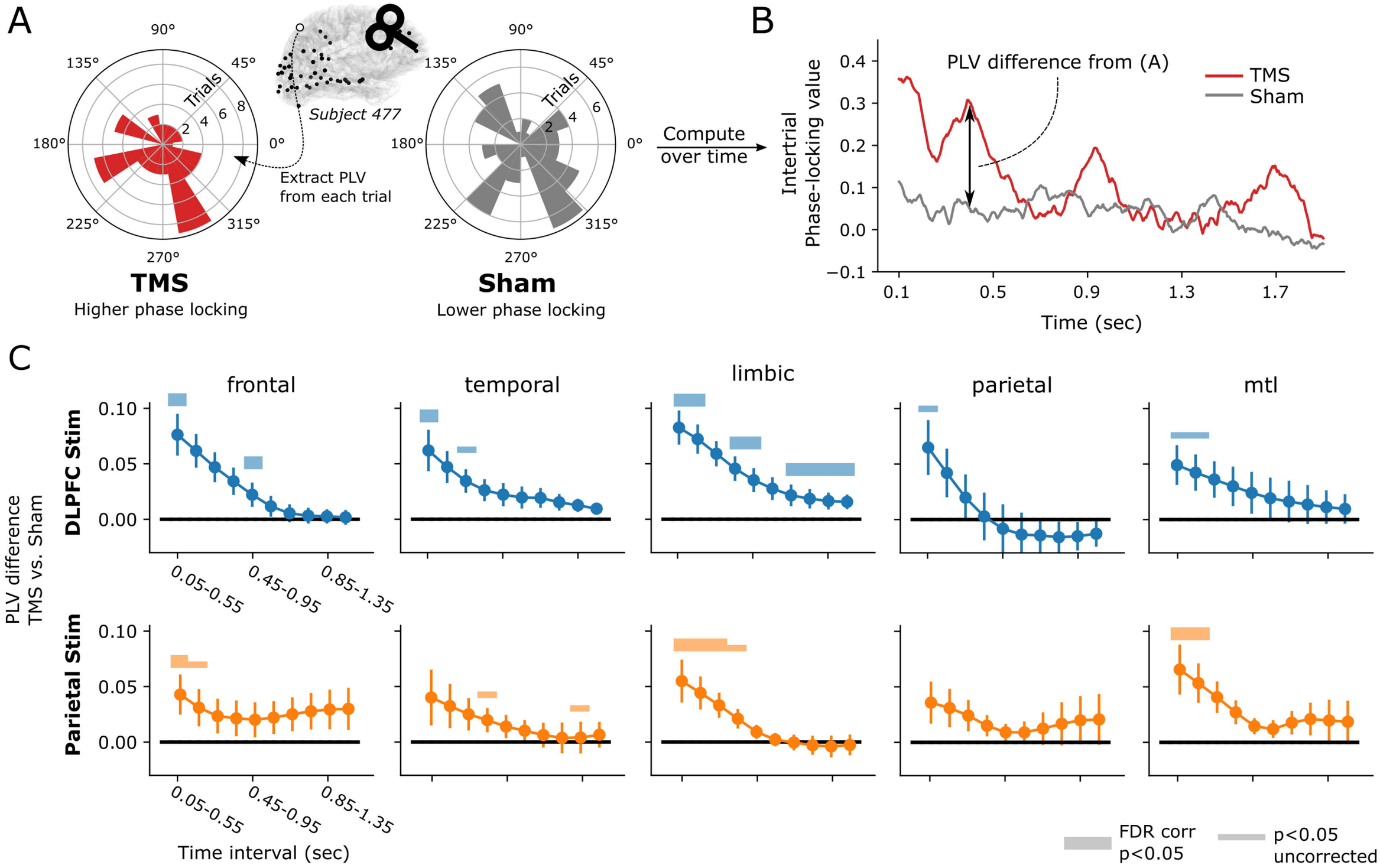
A
90°
135°
45°
180°
0°
225°
315°
270°
Trials
2
4
6
8
TMS
Higher phase locking
Subject 477
Extract PLV
from each trial
Sham
Lower phase locking
Compute
over time
B
PLV difference from (A)
TMS
Sham
Intertrial
Phase-locking value
0.4
0.3
0.2
0.1
0.0
−0.1
0.1
0.5
0.9
1.3
1.7
Time (sec)
C
frontal
temporal
limbic
parietal
mtl
DLPFC Stim
Parietal Stim
PLV difference
TMS vs. Sham
0.10
0.05
0.00
0.05-0.55
0.45-0.95
0.85-1.35
Time interval (sec)
FDR corr
p<0.05
p<0.05
uncorrected